Available online at www.sciencedirect.com
ScienceDirect
Trans. Nonferrous Met. Soc. China 31(2021) 1689−1699
Transactions of Nonferrous Metals Society of China
www.tnmsc.cn

Effect of extrusion ratios on hardness, microstructure, and crystal texture anisotropy in pure niobium tubes subjected to hydrostatic extrusion

Jongbeom LEE[1], Haguk JEONG[1], Sangyong PARK[1,2]

1. Advanced Materials and Process R&D Department, Korea Institute of Industrial Technology, Incheon City, 21999, Korea;
2. Department of Advanced Materials Science and Engineering, Inha University, Incheon City, 22212, Korea

Received 8 July 2020; accepted 30 December 2020

Abstract: Nb tubes were fabricated through hydrostatic extrusion at extrusion ratios of 3.1 and 6.1 at ambient temperature, and then their microstructure, texture, and Vickers hardness were investigated based on electron back-scattered diffraction (EBSD) data. The fraction of low-angle boundaries (LABs) largely decreased with a sharp decrease in mean grain sizes after hydrostatic extrusion and was not proportional to extrusion ratios, assuming that mixed-asymmetrical junctions forming LABs dissociate at high extrusion ratios from the external stress (>981 MPa) with thermal activation by the generated heat. The correlation between grain size and Vickers hardness followed the Hall−Petch relationship despite the texture gradient of the ⟨111⟩ cyclic fiber textural microstructure at low extrusion ratios and the ⟨100⟩ true fiber textural microstructure at high extrusion ratios. The increase in hydrostatic pressure on the Nb tubes contributed to texture evolution in terms of extrusion ratios due to the difference between {110}⟨111⟩ and {112}⟨111⟩ components based on EBSD data.

Key words: niobium tube; hydrostatic extrusion; microstructure characterization; mechanical properties; texture evolution

1 Introduction

Nb tubes are used as superconductive materials, such as NbTi, Nb_3Sn and Nb_3Al, and for MgB_2/Nb/Cu, Nb as diffusion barriers which disturb the chemical reaction between in-situ or ex-situ Mg−B powders and Cu sheath materials [1−4]. The above-mentioned materials are produced by a wire with a diameter of less than 1 mm for use in magnetic resonance imaging (MRI) magnets with a drawing process. To improve the superconductivity of the materials incorporated in Nb tubes, the essential key is to deform the Nb tube to the required wire diameter without cracking it. Nb tubes have a body-centered cubic (BCC) structure. As such, it is important to control the texture evolution to avoid cold brittleness and brittle fracture because these can occur in the directions of dislocation along the crystal lattice ⟨111⟩ in the BCC structure (the commonly active slip systems in a BCC structure are {110}⟨111⟩ and {112}⟨111⟩) [5−7]. Conventional process such as drawing, however, exhibits difficulty in evolving the crystal texture due to the limitation in strain or reduction rate of the low die angle and the area reduction between 5% and 10% [8,9]. It is critical to understand the relationships between individual reduction thickness of the Nb tube and microstructural evolution during deformation to fabricate Nb tubes without fractures or defects. There are only a few studies on thickness reduction of Nb tubes using the drawing processes for one pass because of die angle and low area reduction.

Corresponding author: Jongbeom LEE, E-mail: ljb01@kitech.re.kr
DOI: 10.1016/S1003-6326(21)65608-X

However, the extruding process can be used to produce Nb tubes with various extrusion ratios because the die angle can be varied up to ~90° and a high pressure can be applied to Nb tubes for deformation depending on the specification of the extruding equipment.

Of the extruding processes, the hydrostatic extrusion (HE) method is optimal for fabricating products with a high extrusion ratio and complex shapes because the processing conditions enable the application of uniform pressure on the product. In addition, there is low friction between the product and the container. The desired shape of the material is obtained using tools with special geometries, which prevent the free flow of the material and thereby generate a significant hydrostatic pressure. For instance, Ni single crystals subjected to HE yielded strongly refined microstructures with an average sub grain diameter of approximately 300 nm; HE was realized through sever plastic deformation (SPD) [10] due to external stress and extrusion ratios that are higher than other extrusion processes at ambient temperature [11]. HE was also performed with the aim of applying SPD and refining the grain size to a nanometric scale. Currently, in spite of changes in material dimensions, the HE method is generally classified as an SPD method and recognized as a method of grain refinement for metallic materials because the larger shear strains generate high-density crystal lattice defects, especially dislocations, which can lead to significant grain refinement [12]. It is worth noting that for HE, the friction between the die and the material is significantly reduced due to the hydrostatic medium and the lubricant additionally applied at the outlet of the die. HE results in a product with high surface quality, which is particularly important for fabricating the tube materials [13].

During Nb tube deformation, the microstructure, the texture, and the relationship between neighboring grain boundaries are determined by complex mechanisms [14,15]. These mechanisms include dislocation interactions that result in the formation of sub-grains and in homogeneities, rotation of grains, and preferential grain coarsening, and they contribute to the mechanical properties of Nb tubes, such as the Vickers hardness. Recovery and recrystallization are important mechanisms for grain refinement and for avoiding the crack caused by dislocation. The hydrostatic extrusion experiment was performed at room temperature; therefore, recovery and recrystallization did not induce microstructure evolution due to the high melting temperature of Nb materials (~2750 K). During the HE deformation of Nb tubes, it is expected that the HE process, through SPD, brings about the microstructure and texture evolution of the Nb tube under high hydrostatic pressure at ambient temperature.

This work aims to investigate the effect of extrusion ratios on Vickers hardness, micro-structural evolution, and textural evolution during the hydrostatic extrusion of Nb tubes by increasing the extrusion ratio at ambient temperature.

2 Experimental

Niobium, used in the present study in the form of extruded and subsequently annealed tube, was obtained from Baoji Junuo Metal Co., Ltd. (China). The nominal impurity levels of the used niobium tubes in the starting material are given in Table 1.

Table 1 Chemical composition of as-received Nb tube (wt.%)

Nb	C	N	O	H	Fe	Si
≥99.95	0.003	0.003	≤0.007	0.001	0.002	0.003

The niobium tubes were 40 mm in diameter, 4 mm in thickness, and 200 mm in length. The Nb tube and Al bar exhibited ultimate tensile strengths of 245 MPa and 190 MPa, respectively, at ambient temperature. An aluminum (Al 1100) bar was inserted in the Nb tube to avoid crushing, as depicted in Fig. 1(a), when the pressure of the fluid in the hydrostatic extrusion system (Fig. 1(b)) was increased to the critical stress required by the billet to deform [16]. The front of the billet was spun to fit the extrusion die at 45°, to prevent the spilling of the pressure medium between the die and billet during pressing. A ram diameter of 150 mm, ram speed of 0.2 mm/s, and moly grease (omni−59, Rauh Chemical Co. Ltd, South Korea) were used as the pressure medium for the structure depicted in Fig. 1(b). Hydrostatic extrusion was carried out at ambient temperature. The initial billet with a diameter of 40 mm was hydrostatically extruded to a diameter of 24 and 16 mm in one pass, respectively.

Table 2 lists the outer diameter, inner diameter, thickness, area reduction, and true strain of the Nb tube for the determination of tube extrusion ratio. The tube extrusion ratio (R) of the Nb tube was calculated as the initial cross-sectional area of the Nb tube divided by the cross-sectional area of the final extrusion. The true strain of Nb tubes can be calculated using the following equation:

$$\varepsilon = \ln(A_0/A_f) = \ln R \quad (1)$$

where A_0 and A_f refer to the initial and finial cross-sectional areas of Nb tubes, respectively.

The Nb tubes before and after extrusion were examined using the Vickers hardness (VH) measurement and were observed along the directions parallel and perpendicular to the direction of extrusion, as seen in Fig. 1(c). Here, ED, RD and TD indicate extrusion direction, radial direction, and tangential direction, respectively. The observed areas were in the extruded tube core because the deformed tubes are extremely sensitive to the deformation geometry [17,18]. The microstructure and crystal texture of the samples were characterized using electron backscatter diffraction (EBSD) analysis. The grain orientation was determined using the EBSD technique in combination with high-resolution thermal field emission scanning electron microscopy (FE-SEM; S−4300SE, Hitachi Co. Ltd.). Before and after each deformation, the EBSD maps of both areas were obtained (Fig. 1(c)) by using step scans with steps of 0.25 μm. On one of the internal surfaces, the observation area had dimensions of 200 μm × 200 μm. For the EBSD analysis, the samples were subjected to electro-polishing before fine grinding to ensure that the orientation remained unaffected by the treatment procedure. The image quality of the Kikuchi pattern at each EBSD data point was obtained using the OIM analysis software (TSL Co. Ltd.). A relatively clean image was obtained by utilizing the grain dilution clean-up function with a tolerance of 5°.

3 Results

3.1 Microstructure of tested Nb tube

Figure 2 illustrates the grain boundary maps obtained from EBSD data for the Nb tube before and after the deformation at hydrostatic extrusion ratios of 3.1 and 6.1 at ambient temperature. The grain boundaries measured using EBSD (Fig. 2) were defined as follows: the red lines are low-angle boundaries (LABs, 2°−15°) and the black lines indicate high-angle boundaries (HABs, 15°−65°). The grain size of the Nb tubes decreased before and after hydrostatic extrusion at both normal planes perpendicular and parallel to the extrusion direction. The LABs and HABs were mixed together at the

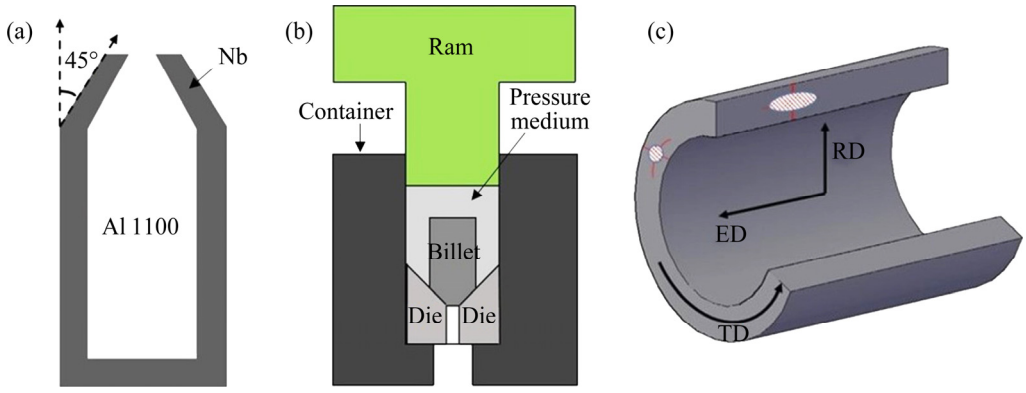

Fig. 1 Schematic diagrams of Nb billet (a), hydrostatic extrusion (b), and area of Vickers hardness measurement and microstructure observation in Nb tube (c) (ED−Extrusion direction; RD−Radial direction; TD−Tangential direction)

Table 2 Variations in thickness, tube area, and strain with extrusion ratio

Sample No.	Outer diameter/mm	Inner diameter/mm	Thickness/mm	Tube area/mm^2	Area reduction/%	Strain	Extrusion ratio
1	40	32	4	452.4	0	0	1
2	25	20.6	2.2	157.6	65.2	1.1	3.1
3	16	12.7	1.65	74.4	83.6	1.8	6.1

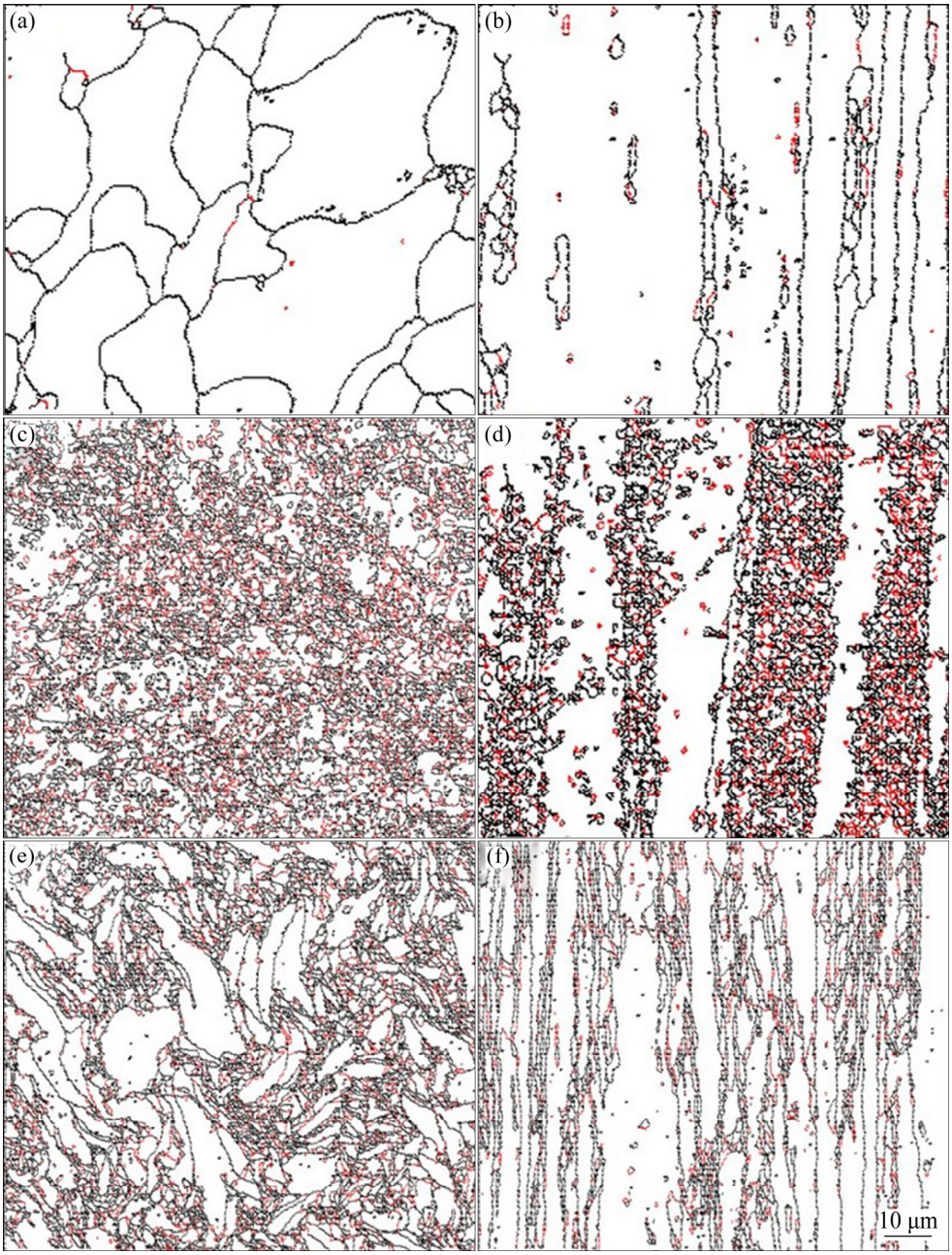

Fig. 2 Grain boundary maps before (a, b) and after deformation at hydrostatic extrusion ratios of 3.1 (c, d) and 6.1 (e, f): (a, c, e) Plane perpendicular to ED; (b, d, f) Plane parallel to ED

extrusion ratio of 3.1; however, the HABs without LABs, as well as the HABs neighboring LABS, were observed at the extrusion ratio of 6.1. The microstructure of the Nb tube varied with the observed planes in terms of extrusion direction. In the normal plane parallel to the extrusion direction (ED) in Figs. 2(c, e), the grain was refined and shaped by circle type at lower extrusion ratios (Fig. 2(c)). On the other hand, at higher extrusion ratios (Fig. 2(e)), the grain sizes were irregular and bent-type shaped grains were observed, which were probably operated by the shear stress along the tangential direction (TD). From the results of the microstructure observation on the normal plane perpendicular to the ED in Figs. 2(d, f), wide bands with width of 10−25 μm, consisting of LABs, were formed at lower extrusion ratio, whereas the narrow bands of ~5 μm in width were arranged at higher extrusion ratios, thereby showing that the tensor mode was operated differently under applied stress by increasing the extrusion ratio.

3.2 Vickers hardness of tested Nb tube

The relationship between the mean grain sizes

and mechanical properties of Nb tubes was investigated using the Vickers hardness measurement. As can be seen from Fig. 3(a), the Vickers hardness increased with decreasing mean grain size of the ND and TD planes in the Nb tube subjected to hydrostatic extrusion. The mean grain size decreased when the extrusion ratio reached 3.1, and then slightly increased at extrusion ratio of 6.1. To increase the mean grain size, it is necessary to identify what needs to be introduced to stimulate it. The variation in the Vickers hardness (H) and mean grain size (d), as shown in Fig. 3(b), is described mathematically by the Hall−Petch equation, which establishes a relationship between the hardness of a material and its flow stress [19,20]:

$$H=H_0+K_H d^{-1/2} \quad (2)$$

where H_0 and K_H are experimental constants. From Fig. 3, H_0 and K_H can be calculated to be 1070.9 MPa and 20.3 MPa·mm$^{1/2}$, respectively, for Nb tubes subjected to hydrostatic extrusion at ambient temperature. The K_H-value varies with the extent of deformation due to dislocation strengthening and high angle boundary strengthening [21]; therefore, K_H (≈2.07 kg·mm$^{-3/2}$) values of this study are twice that (≈1.02 kg·mm$^{-3/2}$) of annealed Nb materials in a previous study [22]. The increase in the K_H-value caused by the work-hardening characteristics is interpreted in terms of the cell formation theory (LABs or sub- grains) of working hardening, which is in good agreement with Fig. 2 showing the increase of LABs fraction after hydrostatic extrusion [23].

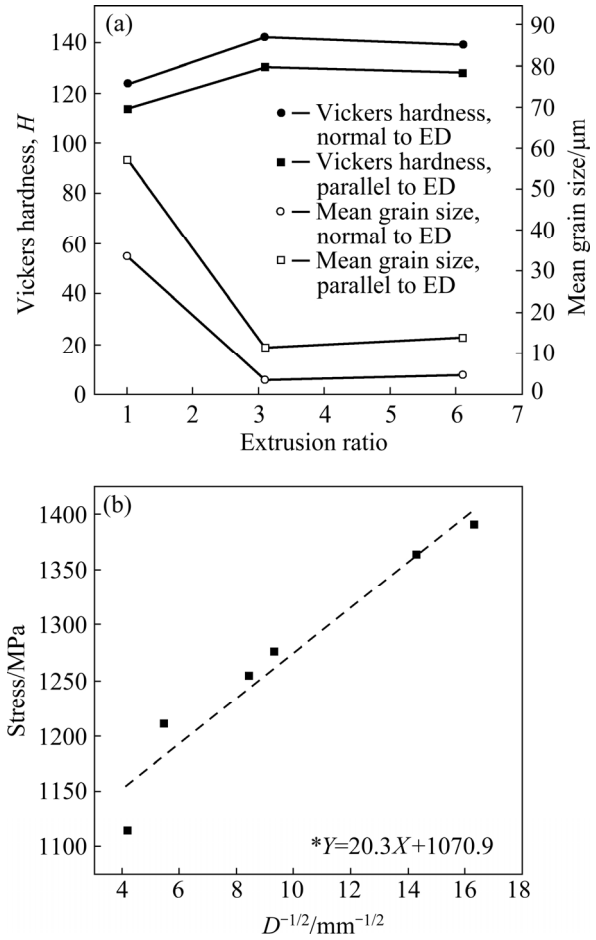

Fig. 3 Change in Vickers hardness and mean grain size vs extrusion ratios (a), and stress vs grain size (b)

3.3 Grain boundary character of tested Nb tube

Figure 4 shows the relation of the fractions of the LABs and HABs against the extrusion ratios in the ED plane and TD planes of Nb tubes. The fraction of LABs increased before and after hydrostatic extrusion, and decreased as the extrusion ratio increased, and vice versa for the HABs. Interestingly, the fraction of LABs and HABs in the ED and TD plane of the Nb tube is analogous, irrespective of extrusion ratios, indicating that dislocations glide on a similar slip system and grains rotate at similar angles in the ED and TD planes during the deformation. LABs are composed of an array of edge dislocation, screw dislocations, and mixed dislocations.

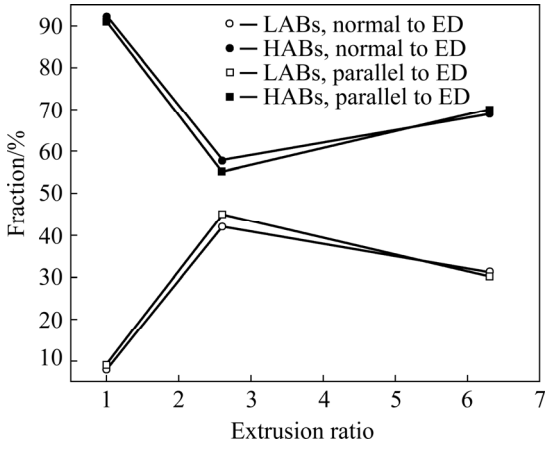

Fig. 4 Variation in LAB and HAB fractions against extrusion ratio in ED and TD planes of Nb tubes

The increase in extrusion ratios produced a strain in the Nb tubes, which resulted in microstructure evolution through plastic strain. The potential use of EBSD is quantifying strain in deformed materials, as the residual strain manifests local variations in lattice orientation. The Kernel average misorientation (KAM) is the average

misorientation among all neighboring points within the kernel. A kernel is a set of points of a prescribed size surrounding the scan point of interest. The merit of KAM is that it focuses on local small rotations because the grain boundary effect is excluded by only including misorientation less than a specified tolerance value from the averaging calculation. If the kernel contains a grain boundary, then the KAM value would be quite large [24]. Figure 5(a) shows the average degrees of KAM values of Nb tubes before and after hydrostatic extrusion. The mean KAM value increased after hydrostatic extrusion through plastic strains. From Fig. 5(a), the mean KAM value for the plane normal to ED is higher than that for the plane parallel to ED, which indicates the differences in the plastic strain at the same extrusion ratio. In addition, the difference in the mean KAM values for both the plane normal and parallel to the ED is larger at low extrusion ratio than at a high extrusion ratio. Therefore, manipulating the identical extent of a plastic strain in terms of directions normal and parallel to the ED can give rise to the Nb tube during deformation by increasing the extrusion ratios. There are areas with net nonzero Burgers vectors across which there is a change in crystallographic orientation or lattice curvature due to extra stress. These dislocations are termed geometrically necessary dislocation (GNDs). Figure 5(b) shows the variation of GND density versus extrusion ratios in terms of the planes normal and parallel to ED. The GND density of the Nb tube largely increased after hydrostatic extrusion, and the plan normal to the ED had a larger value for GND density than the plan parallel to the ED. Interestingly, the difference between both planes at the same extrusion ratios decreased with an increase in the extrusion ratio. It is notable that the fraction of sub grains in Nb tubes can be confined by extrusion ratios because arrays of GNDs can form sub grain boundaries.

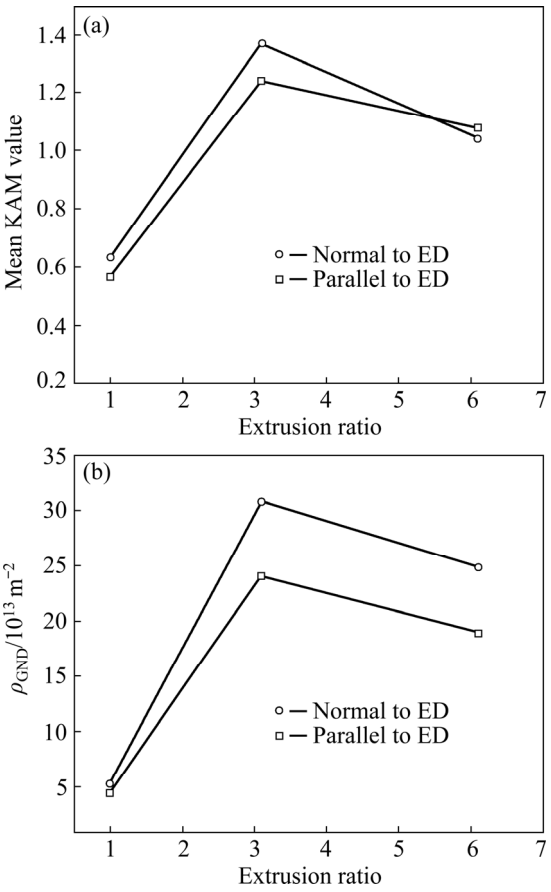

Fig. 5 Variation in mean KAM value (a) and GND density (b) against extrusion ratio in ED and TD planes

3.4 Microtexture of tested Nb tube

Figure 6 depicts the {100} discrete pole figures for the plane parallel to the ED in the Nb before and after hydrostatic extrusion. As can be seen, the type of the pole figure varied with extrusion ratios, and the pole figure for the Nb tube at low extrusion ratios indicated the ⟨111⟩ fiber texture, whereas at high extrusion ratios, the pole figures indicated ⟨100⟩ fiber textures [25]. As can be seen from Figs. 6(b, c), both fiber textures had different types, and they were the so-called cyclic texture (Fig. 6(b)) and true fiber texture (Fig. 6(c)). The texture heterogeneities were observed in the wire, and the texture type varied from cyclic texture to true fiber texture with increasing distance from the wire core because the area adjacent to the wire die was subjected to larger shear stress than the wire core [17]. Such significant variations in texture have also been observed in extruded materials from the surface to the center [26]. It is suggested that increasing the extrusion ratios could exert larger shear stress in Nb tubes during hydrostatic extrusion.

3.5 R_W/R_D measurement of tested Nb tube

Figure 7 shows the variation of the R_W/R_D value as a function of extrusion ratios. Here, R_W is the reduction in wall thickness of the tube, and R_D defines the reduction in tube diameter. R_W and R_D are calculated as follows:

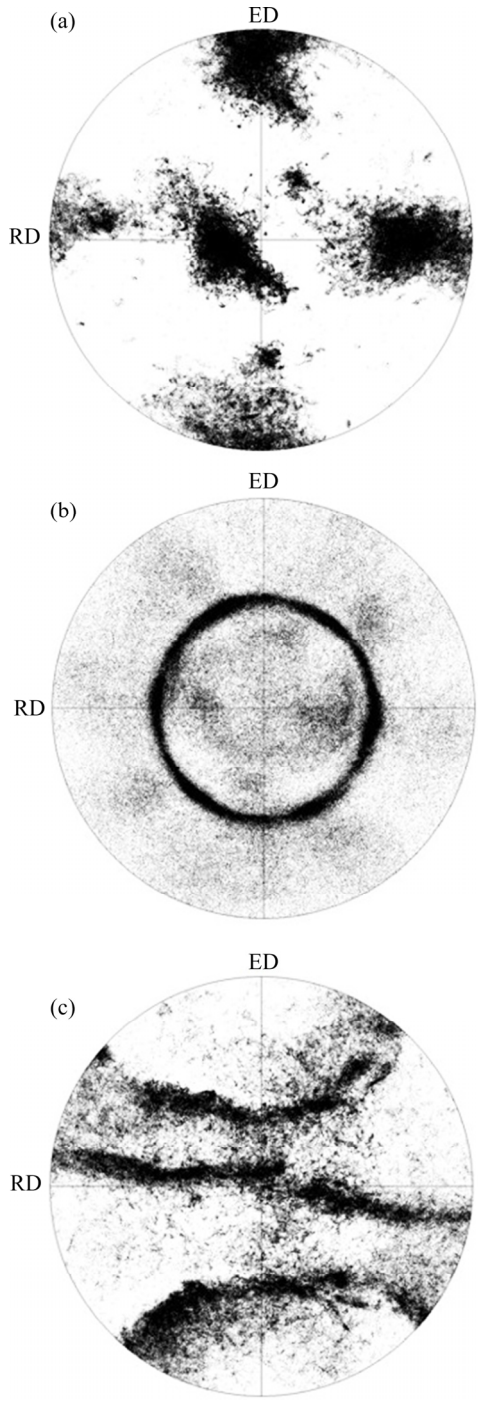

Fig. 6 {100} discrete pole figures for plane parallel to ED in Nb tubes before (a) and after hydrostatic extrusion at extrusion ratios of 3.1 (b) and 6.1 (c)

$$R_{\mathrm{W}}=\frac{t_{\mathrm{i}}-t_{\mathrm{f}}}{t_{\mathrm{i}}} \tag{3}$$

$$R_{\mathrm{D}}=\frac{d_{\mathrm{i}}-d_{\mathrm{f}}}{d_{\mathrm{i}}} \tag{4}$$

where t_{i} and t_{f} are the wall thicknesses of the initial and final tubes, respectively, and d_{i} and d_{f} are the diameters of the initial and final tubes, respectively. The $R_{\mathrm{W}}/R_{\mathrm{D}}$ value is more than 1 at low extrusion ratios and approximately 1 at high extrusion ratio. The reason for applying the above equation is to compare the texture evolution shown in the previous studies using zircaloy tubes with a hexagonal close packed (HCP) structure formed through extrusion and pilgering [17]. As a result, the texture of zircaloy exhibits three separate types according to the $R_{\mathrm{W}}/R_{\mathrm{D}}$ value of more than, less than, and equal to 1. The present study used an Nb tube with the BCC structure to show both distinct types of texture from the $R_{\mathrm{W}}/R_{\mathrm{D}}$ value of more than and equal to 1 at low and high extrusion ratios, respectively. According to Ref. [17], a value of more than 1 indicates that the strain level in the radial direction is larger than that in the tangential direction, and a value of approximately 1 shows that the strain level in the radial direction is analogous to that in the tangential direction, thereby implying that extrusion ratios make it possible to constrain the texture evolution during hydrostatic extrusion.

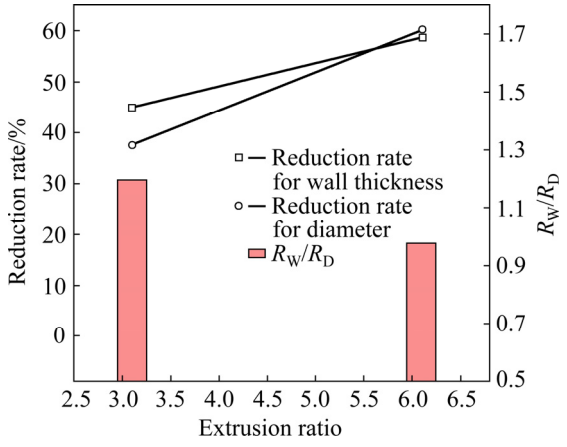

Fig. 7 Variation in $R_{\mathrm{W}}/R_{\mathrm{D}}$ values as function of extrusion ratio

4 Discussion

4.1 Mechanical properties and microstructure evolution

The variation in hardness, microstructure, and texture evolution of the Nb tube were investigated during deformation under hydrostatic extrusion. The microstructure of the Nb tube was refined and the fraction of LABs largely increased after hydrostatic extrusion, and the LABs had different misorientations, as shown in Fig. 7. The texture

evolution of the plane parallel to the ED in Nb tubes was shown by increasing the extrusion ratios. The variation in Vickers hardness with respect to grain size followed the Hall−Petch equation without exhibiting a boundary-hardening effect (Fig. 2) or textural gradient (Fig. 6). In general, the hardening sequence from ⟨111⟩ to ⟨100⟩ and to ⟨110⟩ may result from the difference in atomic distance of Nb materials, respectively, d_{111}=9.5 nm, d_{100}=16.5 nm, and d_{110}=23.3 nm. The Nb tubes subjected to hydrostatic extrusion at various extrusion ratios exhibited the ⟨111⟩ fiber texture at low extrusion ratios and the ⟨100⟩ fiber texture at high extrusion ratios; however, the texture evolution did not contribute to the variation in Vickers hardness (Fig. 6) due to low shear modulus (38 GPa), and then Nb materials have high ductility to fracture and are not susceptible to fracture at room temperature. According to Ref. [27], the physical properties of Nb show that the critical temperature is 290 K, with a thermal contribution of 13 MPa, implying that the lattice resistance to dislocation motion is negligible at room temperature in the Vickers hardness measurement. The phenomenon was also supported by a work [28,29] on uniaxial compression experiments over a wide range of strain (10^{-3}−10^{4} s^{-1}), and Nb materials exhibit excellent ductility and significant thermal softening for the ⟨100⟩ textured polycrystalline both at quasi-static and high-strain rates.

The fraction of LABs was larger at low extrusion ratios than at high extrusion ratios, and the mean grain size increased by increasing the extrusion ratios. It is associated with dislocation interactions and the formation of LABs during deformation. LIU et al [30] reported the correlation of dislocation interactions and low-angle boundary strengthening using discrete dislocation dynamics (DD) simulation. Five different dislocation interaction types are considered: collinear, mixed-symmetrical junction, mixed-asymmetrical junction, edge junction, and coplanar. Of these, mixed-symmetrical junction formation events are found not only to cause a strong resistance against the incident dislocation penetration, but also to transform the symmetrical low-angle tilt grain boundary into a hexagonal network (a general low-angle GB). As a result of the DD simulation, the mixed-symmetrical junctions forming LABs dissociate when the external stress reaches 981 MPa. In the present study, the external stress for hydrostatically extruding the Nb tubes was increased from 629 to 998 MPa by increasing the extrusion ratios from 3.1 to 6.1. Such an increase in external stress could be attributed to the decrease in the LABs fraction and the increase in the mean grain sizes in the Nb tubes caused by increasing the extrusion ratios due to the dissociation of mixed-symmetrical junctions during deformation.

4.2 Microtexture evolution

Texture evolution is associated with the slip system activating the Nb tube during the deformation under hydrostatic extrusion at various extrusion ratios. A change was observed from the ⟨111⟩ fiber textured microstructure to the ⟨100⟩ fiber textured microstructure of Nb tubes with an increase in the extrusion ratios. According to Ref. [31], above 175 K, slip was observed on {110} and {112} planes depending on the temperature, loading direction, and orientation of single crystal of Nb materials. In detail, the kink pair theory presented by SEEGER and HOLZWARTH [32] suggests that at moderate temperature, slip occurs on {112} planes, and that at very low temperatures, slip should occur on {110} planes because of the {110} planes having lower energy barriers than {112} at 0 K. In contrast to the kink pair theory, recent work by CAILLARD [33,34] showed that screw dislocations always move on fundamental {110} planes in the temperature range between 100 and 300 K. The screw dislocation core structure is responsible for the high lattice friction, and thus the temperature and strain rate dependence of plastic deformation in BCC metals [35−37]. Increasing the extrusion ratios in the present study requires more external stress, which leads to an increase in strain rate and heat generation [38,39]. Therefore, the formation of screw dislocation core structure is more likely to occur at high extrusion ratios than at low extrusion ratios. The increase in the fraction of screw dislocations at high extrusion ratios contributes to the formation of LABs less than at low extrusion ratios. Because the screw dislocation line and the Burgers vector are parallel, the dislocation may slip in any plane containing the dislocation, resulting in less LABs formation. The variation of both {110}⟨111⟩ and {112}⟨111⟩ component fractions as a function of tolerance based on EBSD data at low and high extrusion

ratios was investigated, as shown in Fig. 8(a). It can be seen that the fraction of the {112}⟨111⟩ component is higher at low extrusion ratio (Fig. 8(b)) and that of the {110}⟨111⟩ component is higher at high extrusion ratios (Fig. 8(c)) with a tolerance of 30°, implying that much more screw dislocations glide on the {110} plane at high extrusion ratios. TERENTYEV et al [40] have shown that the [100] segment formed in the reaction with a $1/2[\bar{1}11]$ loop does not move easily at room temperature. However, with a sufficiently high stress it spits into 1/2[111] and $1/2[\bar{1}11]$ segments, with the common glide plane $(01\bar{1})$, which is also a possible interpretation of Fig. 8.

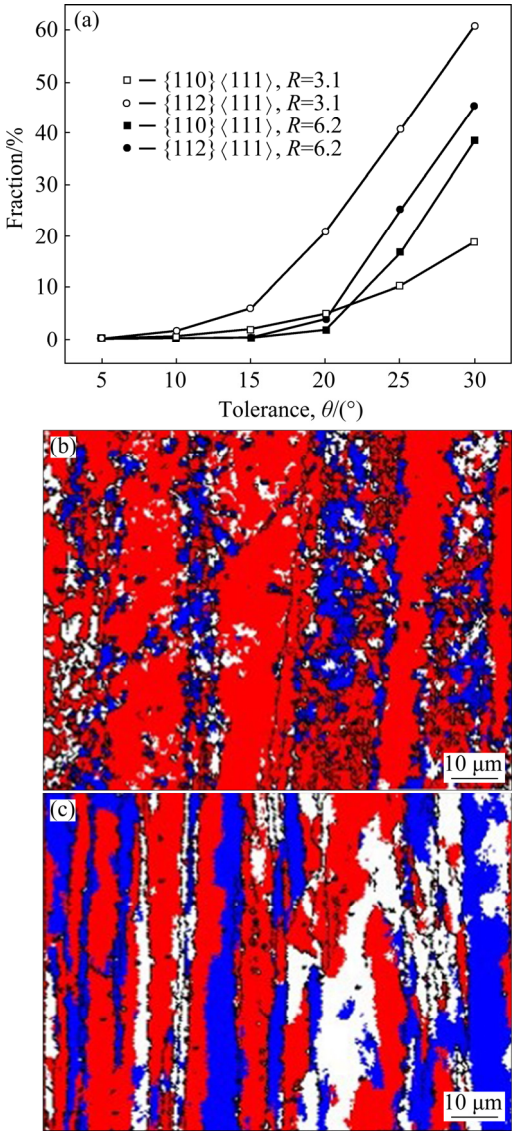

Fig. 8 Variation in texture component fractions as function of tolerance (a), and texture component maps at extrusion ratio of 3.1 (b) and 6.2 (c) with tolerance of 30° (The red and blue colors indicate {112}⟨111⟩ and {110}⟨111⟩, respectively)

5 Conclusions

(1) The fraction of LABs largely decreased with a sharp decrease in mean grain sizes after hydrostatic extrusion and was not proportional to the extrusion ratios. It is assumed that mixed-asymmetrical junctions forming LABs dissociate at high extrusion ratios because of the external stress (>981 MPa) with thermal activation from generated heat.

(2) The correlation between grain size and Vickers hardness followed the Hall−Petch relationship despite the texture gradient. The ⟨111⟩ cyclic fiber textural microstructure was developed at low extrusion ratios and ⟨100⟩ true fiber textural microstructure was evaluated at high extrusion ratios, although the hardening sequence of BCC structural material is from ⟨111⟩ to ⟨100⟩ because of atomic distance, due to being negligible for the lattice resistance to dislocation motion above room temperature.

(3) The increase in hydrostatic pressure on Nb tubes contributed to texture evolution in terms of extrusion ratios due to the difference between {110}⟨111⟩ and {112}⟨111⟩ components based on EBSD data.

Acknowledgments

This study was supported by a Grant from the Fundamental R&D Program (10067694) funded by the Ministry of Trade, Industry and Energy, Korea.

References

[1] LI Y Z. Thermal properties of NbTi superconductor wire and its heat release performance over quench [J]. Materials and Science Engineering A, 2000, 292: 194−197.

[2] ECHARRI A, SPADONI M. Superconducting Nb_3Sn: A review [J]. Cryogenics, 1971, 11: 274−284.

[3] WILLENS R H, GEBALLE T H, GOSSARD A C, MAITA J P, MENTH A, HULL G W Jr, SODENR R. Superconductivity of Nb_3Al [J]. Solid State Communications, 1969, 7: 837−841.

[4] JIE H, QIU W, BILLAH M, MUSTAPIC M, PATEL D, MA Z, GAJDA D, MORAWSKI A, CETNER T, SHAHABUDDIN M, YANMAZ E, RINDFLEISCH M, KIM J H, SHAHRIAR A, HOSSAIN M D. Superior transport J_C obtained in in-situ MgB_2 wires by tailoring the starting materials and using a combined cold high pressure densification and hot isotatic pressure treatment [J]. Scripta Materialia, 2017, 129: 79−83.

[5] CHERNOV V M, KARDASHEV B K, MOROZ K A. Low-temperature embrittlement and fracture of metals with different crystal lattice-dislocation mechanisms [J]. Nuclear Materials and Energy, 2016, 9: 496−501.

[6] MITCHELL T E. Slip in body-centered cubic crystals [J]. Philosophical Magazine, 1968, 17: 1169−1194.

[7] PRIESTNER R, LESLIE W C. Nucleation of deformation twins at slip plane intersections in B.C.C. metals [J]. Philosophical Magazine, 1965, 11: 895−916.

[8] KARABOGA F, ULGEN A T, YETIS H, AKDOGAN M, PAKDIL M, BELENLI I. Mechanical properties and uniformity of Fe−MgB_2 wires upon various wire drawing steps [J]. Materials Science and Engineering A, 2018, 721: 89−95.

[9] JIANG Yan-bin, LI Yong-shuai, LEI Yu, XIE Jian-xin. Cross-sectional structure, microstructure and mechanical property evolutions of brass cladding pure copper stranded wire composite during drawing [J]. Transactions of Nonferrous Metals Society of China, 2020, 30: 1857−1872.

[10] ROGACHEV S O, NIKULIN S A, KHATKEVICH V M, SUNDEEV R V, KOZLOV D A. High-pressure torsion deformation process of bronze/niobium composite [J], Transactions of Nonferrous Metals Society of China, 2019, 29: 1689−1695.

[11] ZDUNEK J, MIZERA J, WASIK K, KURZYDLOWSKI K J, Microstructural analysis of the ⟨111⟩ and ⟨110⟩ nickel single crystals subjected to severe plastic deformation by hydroextrusion [J]. Materials Science and Engineering A, 2013, 569: 92−95.

[12] VALIEV R Z, ISLAMGALIEV R K, ALEXANDROV I V. Bulk nanostructured materials from severe plastic deformation [J]. Progress in Materials Science, 2000, 45: 103−189.

[13] MAJ P, ADAMCZYK-CIESLAK B, MIZERA J, PACHLA W, KURZYDLOWSKI K J. Microstructure and mechanical properties of duplex stainless steel subjected to hydrostatic extrusion [J]. Materials Characterization, 2014, 93: 110−118.

[14] GILL SEVILLANO J, van HOUTTE P, AERNOUDT E. Large strain work hardening and textures [J]. Progress in Materials Science, 1981, 25: 69−134.

[15] LEE J, JEONG H. Effect of rolling speed on microstructural and microtextural evolution of Nb tubes during caliber-rolling process [J]. Metals, 2019, 9: 500. DOI: 10.3390/met9050500.

[16] INOUE N, NISHIHARA M. Hydrostatic extrusion theory and applications [M]. New York: Elsevier, 1985.

[17] TENCKHOOF H. Deformation mechanisms, texture and anisotropy in zirconium and zircaloy [M]. Philadelphia (PA): ASTM, 1998.

[18] WU Yi-ping, XIONG Han-qing, JIA Yu-zhen, XIE Shao-hui, LI Guo-feng. Microstructure, texture and mechanical properties of Mg−8Gd−4Y−1Nd−0.5Zr alloy prepared by pre-deformation annealing, hot compression and aging [J]. Transactions of Nonferrous Metals Society of China, 2019, 29: 976−983.

[19] HALL E O. The deformation and ageing of mild steel: III Discussion of results [C]//Proceedings of the Physical Society: Section B, 1951: 747−752.

[20] ARMSTRONG R W, CODDI, DOUTHWAITER M, PETCHN J. The plastic deformation of polycrystalline aggregates [J]. Philosophical Magazine, 1962, 7: 45−58.

[21] HANSEN N. Hall−Petch relation and boundary strengthening [J]. Scripta Materialia, 2004, 51: 801−806.

[22] OMARA M, ENTWISLEA R. The effect of grain size on the deformation of niobium [J]. Materials Science and Engineering, 1970, 5: 263−270.

[23] MITCHELL T E, FOXALLR A, HIRSCHP B. Work-hardening in niobium single crystals [J]. Philosophical Magazine, 1963, 8: 1895−1920.

[24] LEHOCKEY E M, LIN Yang-pi, LEPIKO E. Mapping residual plastic strain in materials using electron backscatter diffraction [M]//SCHWARTZ A J, KUMAR M, ADAMS B L. Electron Backscatter Diffraction in Materials Science. Boston: Springer, 2000.

[25] CHULIST R, CZERNY M, PANIGRAHIA, ZEHETBAUERM, SCHELLN, SKROTZKIW. Texture and microstructure of HPT-processed Fe-based shape memory alloys [J]. IOP conference Series: Materials Science and Engineering, 2018, 375: 012006.

[26] KHADYKO M, DUMOULIN S, HOPPERSTAD O S. Texture gradients and strain localisation in extruded aluminum profile [J]. International Journal of Solids and Structures, 2016, 15: 239−255.

[27] SUZUKI T, KOIZUMI H, KIRCHNERH O K. Plastic flow stress of b.c.c. transition metals and the peierls potential [J]. Acta Metallurgica et Materialia, 1995, 43: 2177−2187.

[28] SUBHASH G, LEEY J, RAVICHANDRAN G. Plastic deformation of CVD textured tungsten, part I: Constitutive response [J]. Acta Metallurgicaet Materialia, 1994, 42: 319−330.

[29] SUBHASH G, LEE Y J, RAVICHANDRAN G. Plastic deformation of CVD textured tungsten, part II: Constitutive response [J]. Acta Metallurgica et Materialia, 1994, 42: 331−340.

[30] LIU B, RAABE D, EISENLOHR P, ROTERS R, ARSENLIS A, HOMMES G. Dislocation interactions and low-angle grain boundary strengthening [J]. Acta Materialia, 2011, 59: 7125−7134.

[31] FOXALL R A, DUESBERYM S, HIRSCH P B. The Deformation of niobium single crystals [J]. Canadian Journal of Physics, 1967, 45(2): 607−629.

[32] SEEGER A, HOLZWARTH U. Slip planes and kink properties of screw dislocations in high-purity niobium [J]. Philosophical Magazine, 2006, 86: 3861−3892.

[33] CAILLARD D. Kinetics of dislocations in pure Fe. Part 1: In situ straining experiments at room temperature [J]. Acta Materialia, 2010, 58: 3493−3503.

[34] CAILLARD D. Kinetics of dislocations in pure Fe. Part 2: In situ straining experiments at room temperature [J]. Acta Materialia, 2010, 58(9): 3504−3515.

[35] DUESBERY M S, VITEK V. Plastic anisotropy in b.c.c. transition metals [J]. Acta Materialia, 1998, 46: 1481−1492.

[36] DUESBERY M S, RICHARDSONG Y. The dislocation core in crystalline materials [J]. Critical Reviews in Solid State and Materials Sciences, 1991, 17: 1−46.

[37] VITEK V. Theory of the core structures of dislocations in BCC metals [J]. Crystal Lattice Defects, 1974, 5: 1−34.

[38] KAPOOR R, NEMAT-NASSER S. Determination of temperature rise during high strain rate deformation [J]. Mechanics of Materials, 1998, 27: 1−12.
[39] LEE Jongbeom, JEONG Haguk, PARK Sangyong. Effect of extrusion ratios on microstructural evolution, textural evolution, and grain boundary character distributions of pure copper tubes during hydrostatic extrusion [J]. Materials Characterization, 2019, 158: 109941.
[40] TERENTYEV D A, OSETSKYY N, BACOND J. Effects of temperature on structure and mobility of the ⟨100⟩ edge dislocation in body-centered cubic iron [J]. Acta Materialia, 2010, 58: 2477−2482.

挤压比对静液挤压纯铌管硬度、显微组织和晶粒织构各向异性的影响

Jongbeom LEE[1], Haguk JEONG[1], Sangyong PARK[1,2]

1. Advanced Materials and Process R&D Department, Korea Institute of Industrial Technology, Incheon City, 21999, Korea;
2. Department of Advanced Materials Science and Engineering, Inha University, Incheon City, 22212, Korea

摘　要：在室温下采用静液挤压法制备挤压比为 3.1 和 6.1 的铌管，利用电子背散射衍射(EBSD)研究铌管的显微组织、织构和维氏硬度变化。静液挤压后，小角度晶界(LABs)分数随平均晶粒尺寸的急剧减小而大幅降低，且与挤压比不成正比，可能是因为形成 LABs 的混合非对称晶界在高挤压比下由于外部应力(>981 MPa)和因发热产生的热活化而分解。尽管在低挤压比下的⟨111⟩环状纤维织构和在高挤压比下的⟨100⟩纤维织构显微组织的织构梯度不同，晶粒尺寸与维氏硬度之间的关系仍遵循 Hall−Petch 公式。根据 EBSD 数据，在不同挤压比下{110}⟨111⟩和{112}⟨111⟩含量存在差异，因此，Nb 管所受静液压力的增加促进织构的演变。

关键词：铌管；静液挤压；显微组织表征；力学性能；织构演变

(Edited by Bing YANG)